(G)   Numerical and Experimental Results

To begin, we shall show some data of

R. D. Moser, J. Kim & N. N. Mansour, "Direct numerical simulation of turbulent

flow up to $Re_\tau = 590$," Phys. Fluids **11** 943-945 (1999)

as analyzed by Panton (2005). The first figure shows data for $g_0(y^+)$ and the second for the

composite expansion of the stress

$$-\left.\frac{\overline{u'v'}}{u_*^2}\right|_{\text{comp}} = g_0(y^+) - \eta$$

compared with the data. The third compares the composite expansion for the mean velocity

$$\left.\frac{\bar{u}(y)}{u_*}\right|_{\text{comp}} = f_0(y^+) + W_0(\eta)$$

directly with the data and, in the fourth plot, by the log-law "diagnostic function"

$$y^+ \left.\frac{\partial(\bar{u}/u_*)}{\partial y^+}\right|_{\text{comp}} = y^+ \frac{df_0(y^+)}{dy^+} + \eta \frac{dW_0(\eta)}{d\eta}$$

The expansions work less well for the mean-velocity which is not as highly constrained by the

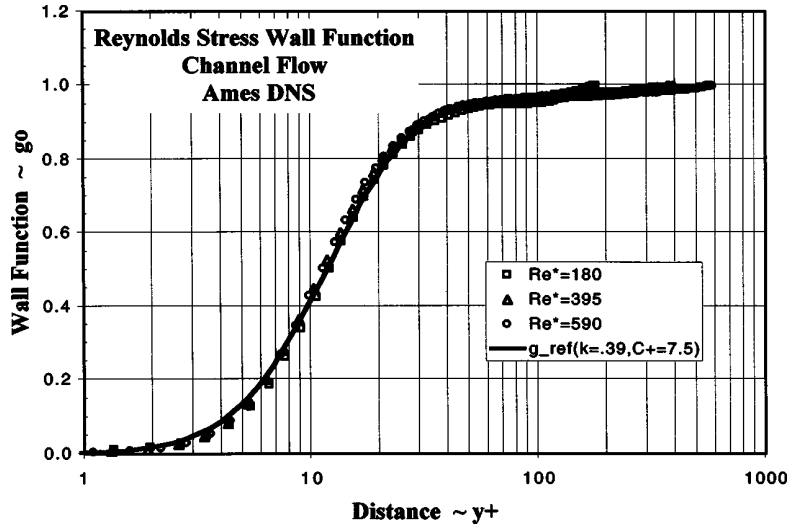RANS equations as in the stress.

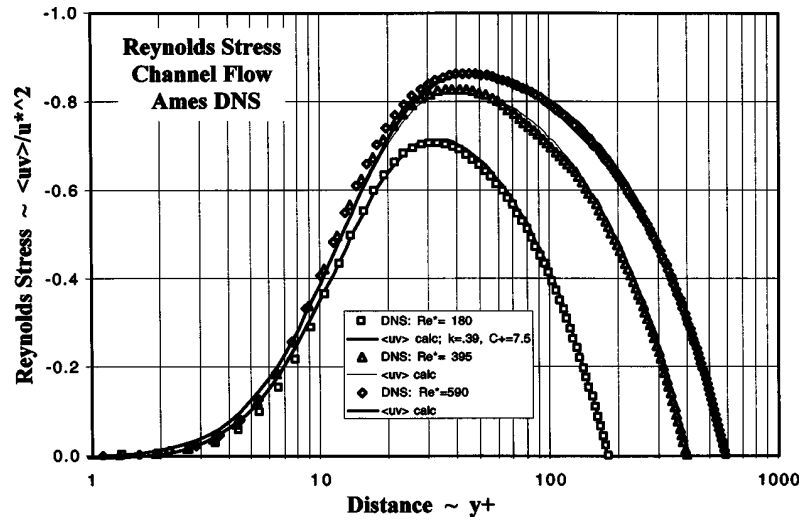Fig. 39 Reynolds stress wall function for Ames channel flow DNS.

.

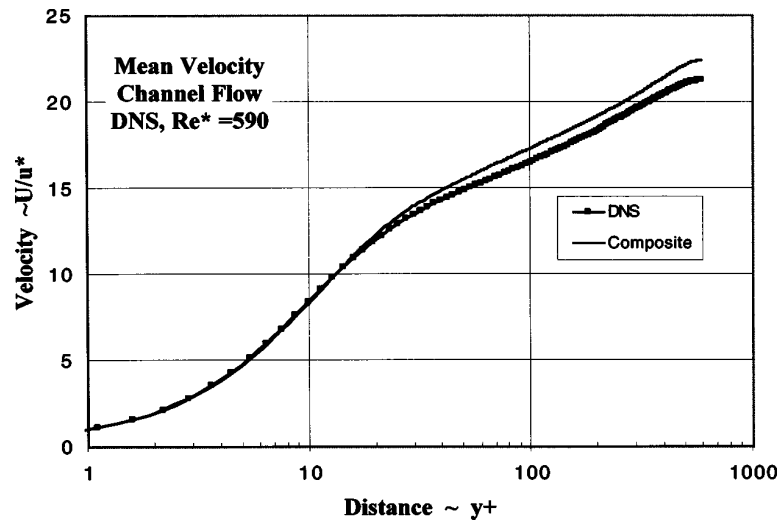Fig. 40 Composite expansion for Reynolds stress and Ames channel flow DNS.

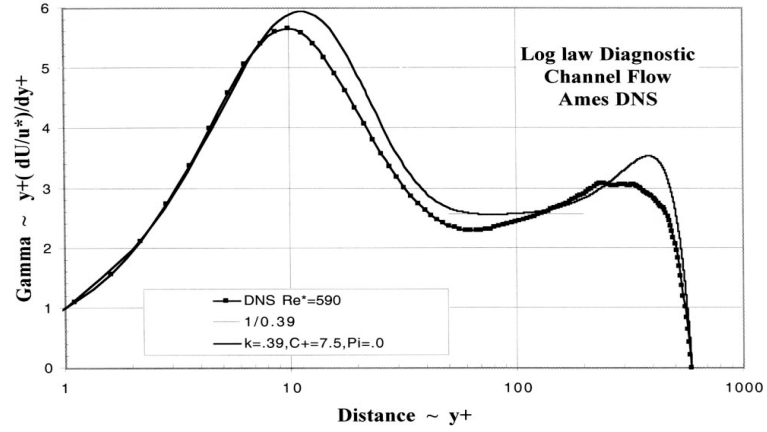Fig. 41 Composite expansion for velocity and Ames channel flow DNS at $Re^*=590$.

Fig. 42 Log law diagnostic function gamma for channel flow. Composite expansion and Ames DNS at Re*=590.

The same quantity has been analyzed in more recent simulations of

> S. Hoyas & J. Jiménez, "Scaling of the velocity fluctuations in turbulent channels up to $Re_\tau = 2003$," Phys. Fluids **18** 011702 (2006)

by

> J. Jiménez & R. D. Moser, "What are we learning from simulating wall turbulence?" Philos. Trans. Roy. Soc. A **365** 715-732 (2007).

In the first figure, the diagnostic function is plotted in both inner and outer scalings. No clear plateau is observed. In the second figure a comparison is made with the next-order matched asymptotics of

> N. Afzal & K. Yajnik, "Analysis of turbulent pipe and channel flows at moderately large Reynolds number," J. Fluid Mech. **61** 23-31 (1973)

which leads to the prediction

$$y\frac{\partial(\bar{u}/u_*)}{\partial y} = \frac{1}{\kappa} + \alpha\frac{y^+}{Re_*} + \frac{\beta}{Re_*}$$

or

$$y\frac{\partial(\bar{u}/u_*)}{\partial y} = \frac{1}{\kappa} + \alpha\eta + \frac{\beta}{Re_*}$$

63

The agreement seems good with $\alpha = 1.0, \beta = 150$, when compared with the DNS and also experiments of

V. K. Natrajan & K. T. Christansen, "The role of coherent structures in subgrid-scale energy transfer within the log-layer of wall turbulence," Phys. Fluids **18** 065104 (2006)
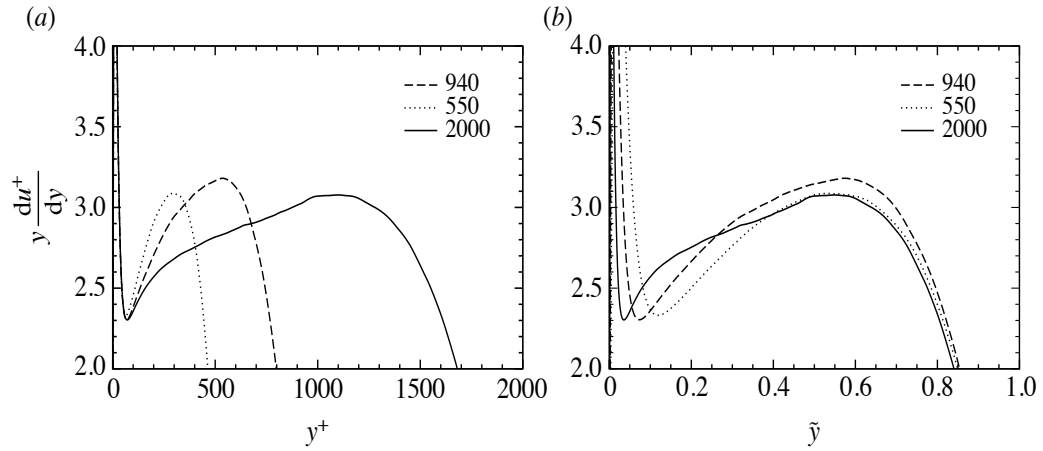

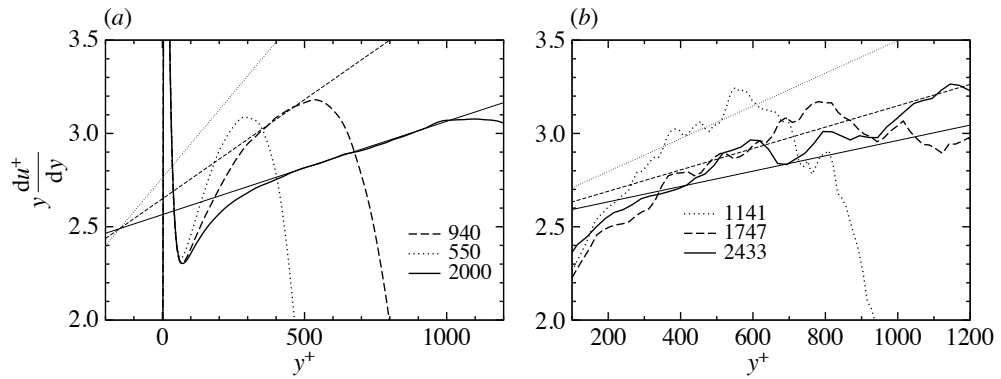Figure 6. $y\mathrm{d}u^+/\mathrm{d}y$ from direct numerical simulation at $h^+ = 550$, 940 and 2000.

Figure 7. Zoomed-in view of $y(\mathrm{d}u^+/\mathrm{d}y)$ from (a) direct numerical simulation for Reynolds numbers $h^+ = 550$, 940 and 2000 and (b) PIV measurements at Reynolds numbers $h^+ = 1141$, 1747 and 2433. The thin lines are $y(\mathrm{d}u^+/\mathrm{d}y)$ determined from equation (4.8), with constants $\alpha = 1.0$, $\beta = 150$ and $1/\kappa = 2.49$, which were determined from the simulation data in (a).

But note that an overlap region seems to exist only for $Re_* \gtrsim 900$ and for $y^+ \gtrsim 300$!

We next consider data from the Princeton Superpipe experiment which studied turbulent pipe-flow over a broad range of Reynolds numbers $Re = 3 \times 10^3 - 35 \times 10^6$. The results on the mean-flow velocity are reported in

M. V. Zagarola & A. J. Smits, "Mean-flow scaling of turbulent pipe flow," J. Fluid Mech. **373** 33-79 (1998)

with some important quantitative corrections in

B. J. McKeon et al. "Further observations on the mean velocity distribution in fully developed pipe flow," J. Fluid Mech. **501** 135-147 (2004)
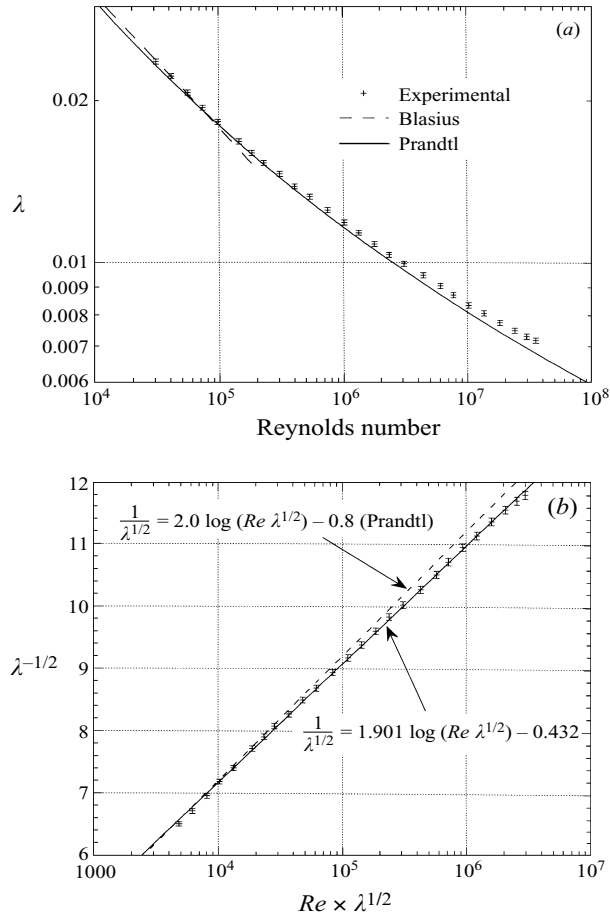
FIGURE 9. A comparison between our friction factor data with the relations proposed by (*a*) Prandtl and Blasius, (*b*) by Prandtl.

The first figure (above) shows the results on the friction factor $\lambda = 8(u_*/\bar{u}_m)^2$, which are well-described by the Prandtl logarithmic friction law (with modified coefficient). The next figure (below) shows the velocity profiles in inner scaling for 13 different Reynolds numbers.
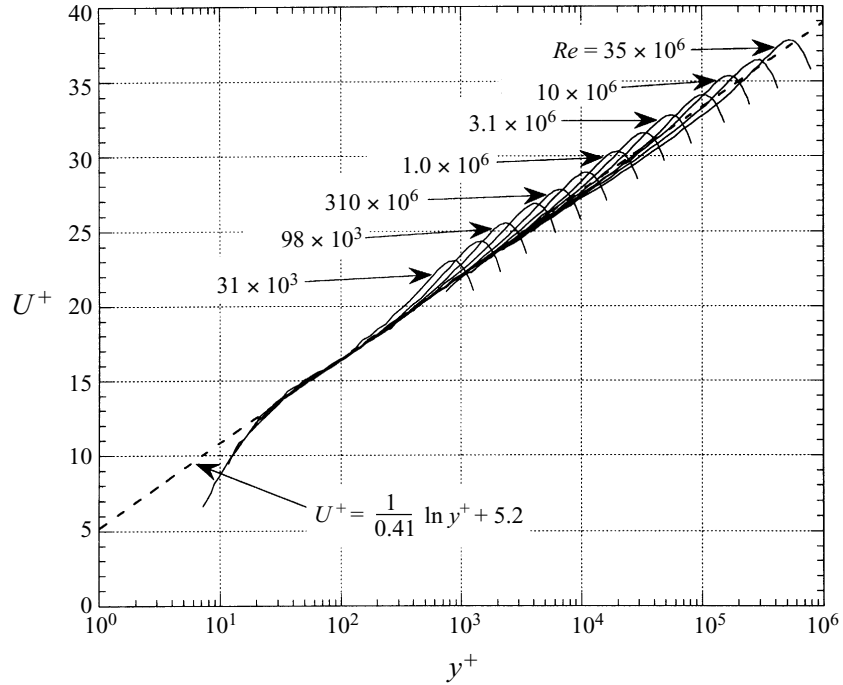
FIGURE 14. A comparison of the velocity profiles normalized using inner scaling variables for 13 different Reynolds numbers between 31×10^3 and 35×10^6.

We next show the results for

$$\Psi \equiv \bar{u}/u_* - \frac{1}{\kappa} \ln y^+$$

with the value of κ inferred from the friction law, $\kappa = 0.436$. This quantity should equal the constant B in the logarithmic region. A plateau is observed in the range

$$600 < y^+ < 0.07 R^+,$$

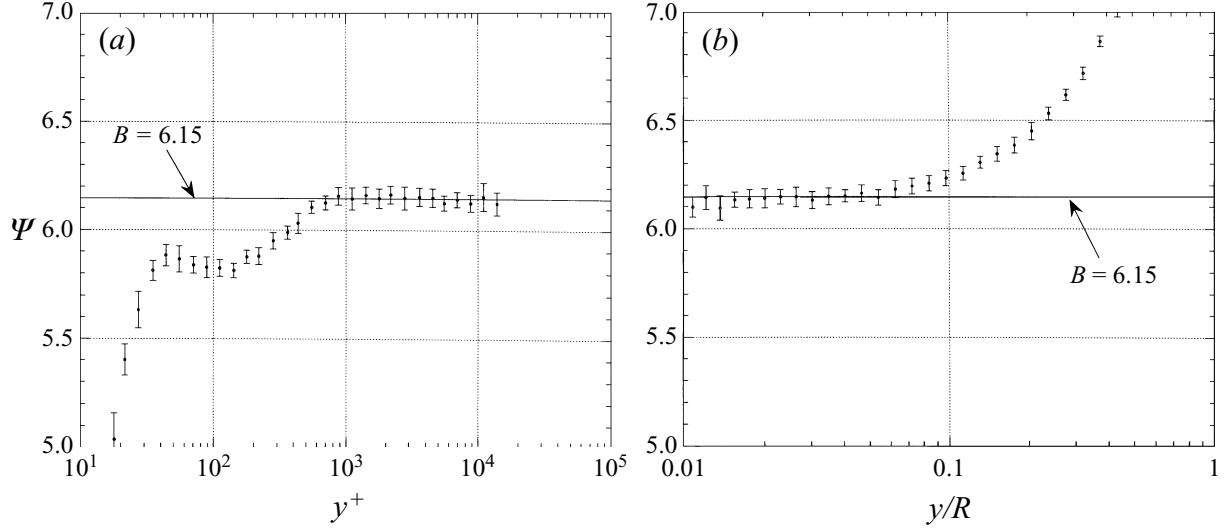smaller than was previously expected.

FIGURE 15. The difference between the velocity profile and the log law as a function of wall-normal position for $\kappa = 0.436$. The value of Ψ was averaged over multiple Reynolds numbers. In (a) the wall-normal positions are normalized using inner scaling variables, and in (b) outer scaling variables.

The next figures show that no choice of κ succeeds to extend the plateau to $y^+ < 600$ and that the region is better fit by a power-law

$$\bar{u}/u_* = 8.70(y^+)^{0.137}.$$

The outer range of the power-law is found to be

$$y^+ = \min\{500, 0.15R^+\}$$

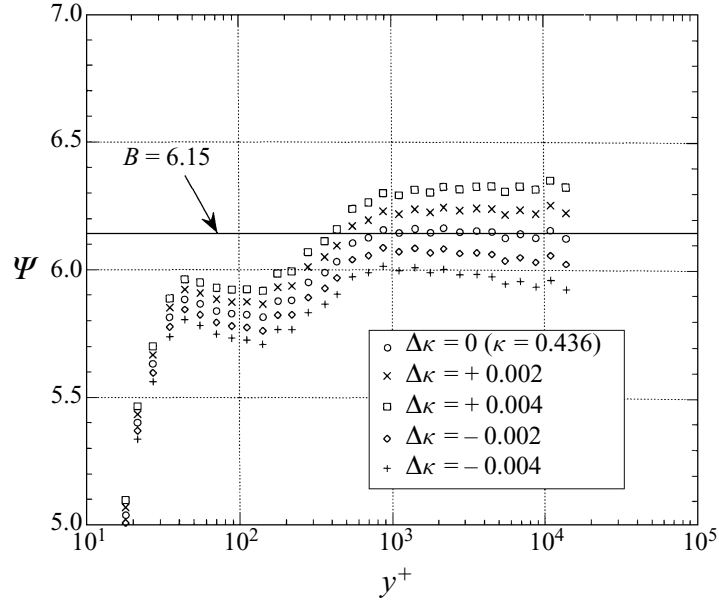so that the range does not grow for $Re_* > 3300$.

FIGURE 16. The difference between the velocity profile and the log law as a function of wall-normal position for different values of κ. The value of Ψ was averaged over multiple Reynolds numbers.
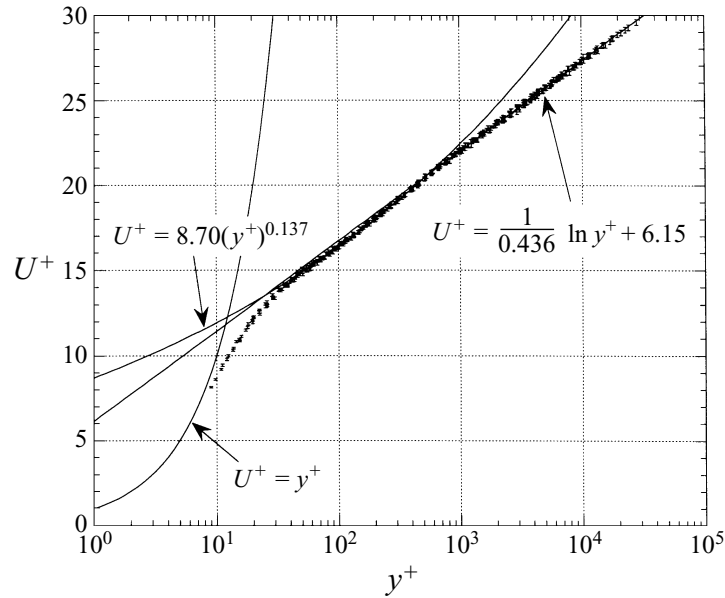

FIGURE 17. A linear–log plot of the velocity profile data within $0.07R^+$ of the wall normalized using inner scaling variables for 26 different Reynolds numbers from 31×10^3 to 35×10^6.
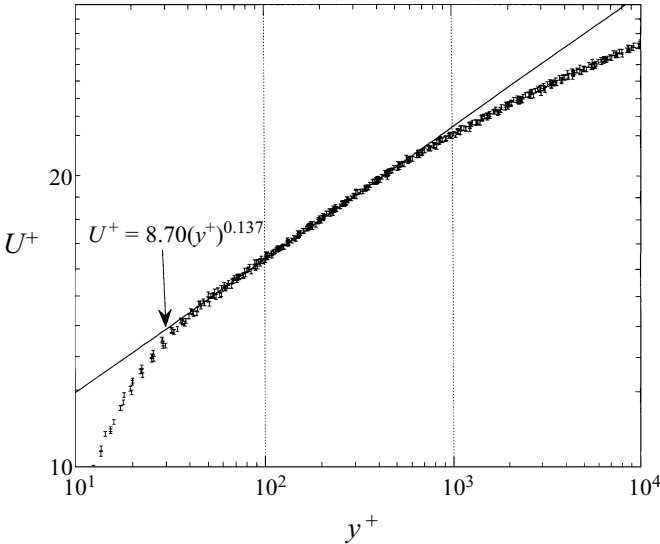
FIGURE 19. A log–log plot of the velocity profile data within $0.07R^+$ of the all normalized using inner scaling variables for 26 different Reynolds numbers from 31×10^3 to 35×10^6.
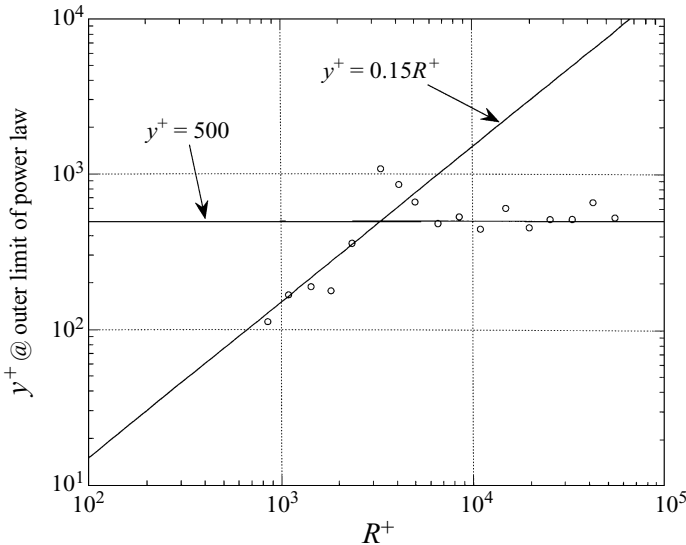
FIGURE 20. The outer limit of the power law region as a function of Reynolds number.

Finally, we present some results of Zagarola & Smits (1998) on outer scaling. They found that $(\bar{u}_c - \bar{u}_m)/u_* \to$ const. as $Re \to \infty$, consistent with standard theory. On the other hand, better collapse in outer scaling was obtained by using $\bar{u}_c - \bar{u}_m$ as the velocity scale rather than the conventional quantity u_*.
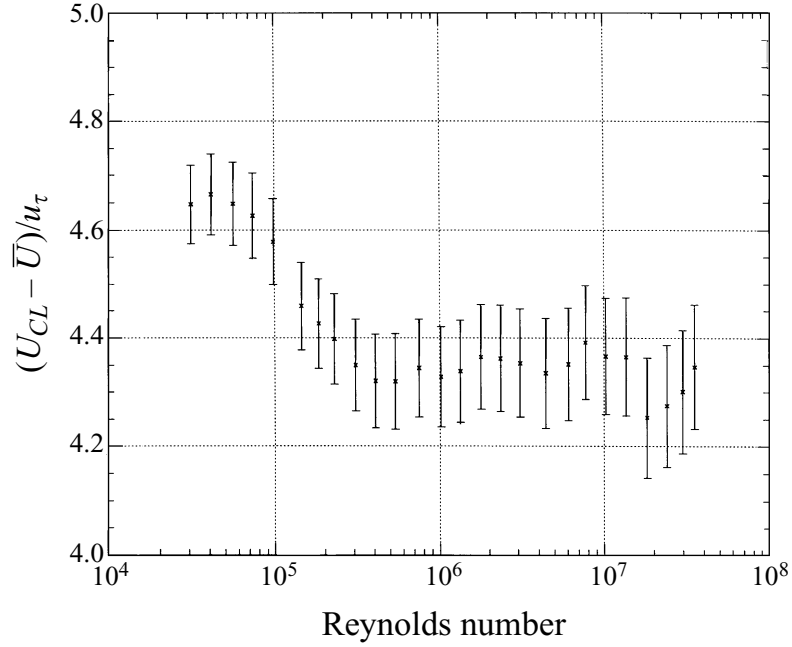
Mean-flow scaling of turbulent pipe flow 69

FIGURE 22. The difference between the average and centreline velocity as a function of Reynolds number.

M. V. Zagarola and A. J. Smits
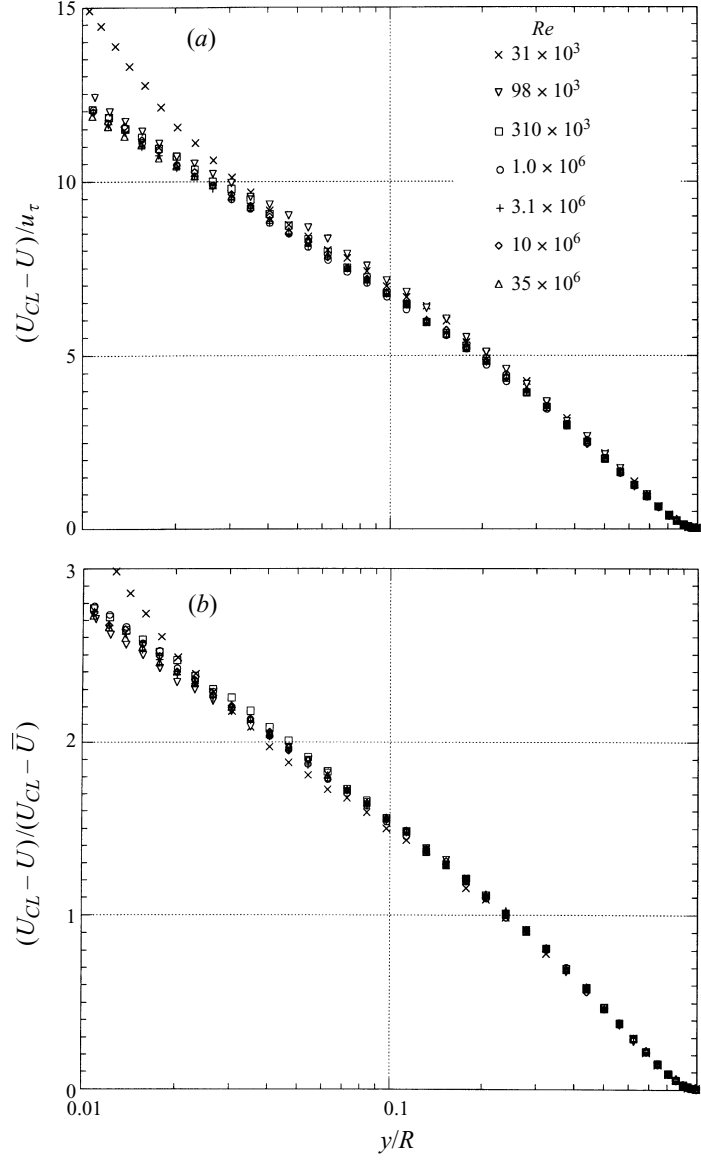

FIGURE 23. A comparison between the velocity profiles normalized by (*a*) u_τ and (*b*) $U_{CL} - \bar{U}$ for Reynolds numbers between 31×10^3 and 35×10^6.

We now consider more results from the Superpipe experiments in

M. V. Zagarola, A. E. Perry & A. J. Smits, "Log laws or power laws: the scaling in the overlap region," Phys. Fluids **9** 2094-2100 (1997)

which tested the Barenblatt-Chorin theory. As seen from the first figure, the BC theory (with constants fit from the old data of Nikuradze) has a decreasing less good fit at increasing Reynolds numbers. Fitting a power law to their data over the range $40 < y^+ < 0.85R^+$, the authors found a best fit as $\bar{u}/u_* = Cy_+^\alpha$ with

$$\alpha = \frac{1.085}{\ln Re} + \frac{6.535}{(\ln Re)^2}$$

$$C = 0.1053(\ln Re) + 0.3055.$$

These power-laws gave a reasonable fit to the data, but with larger fractional differences than a fit by a log-law, especially at higher Reynolds numbers.
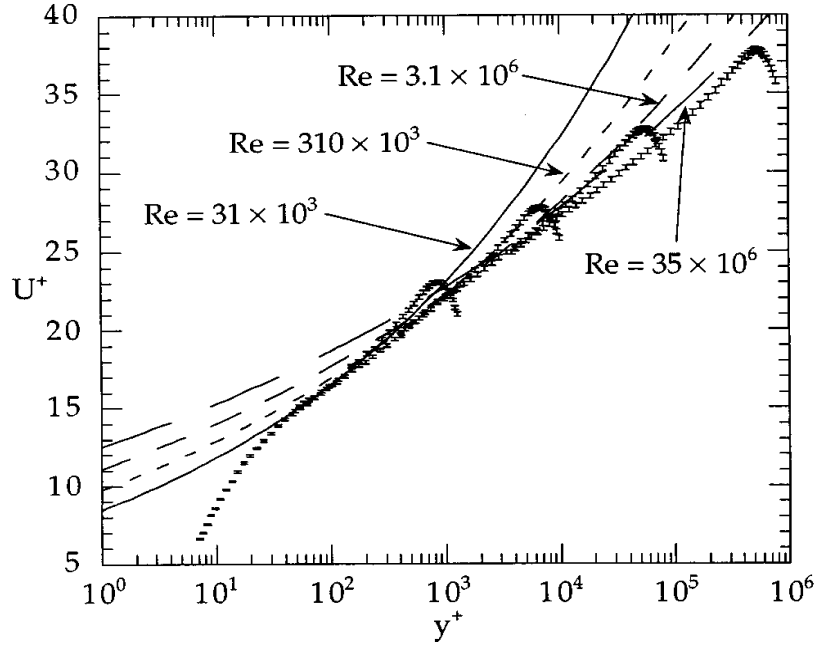

FIG. 5. Comparison between the mean velocity profiles and Eq. (14) for 4 different Reynolds numbers between 31×10^3 and 35×10^6. The error bars represent an uncertainty in U^+ of $\pm 0.57\%$.
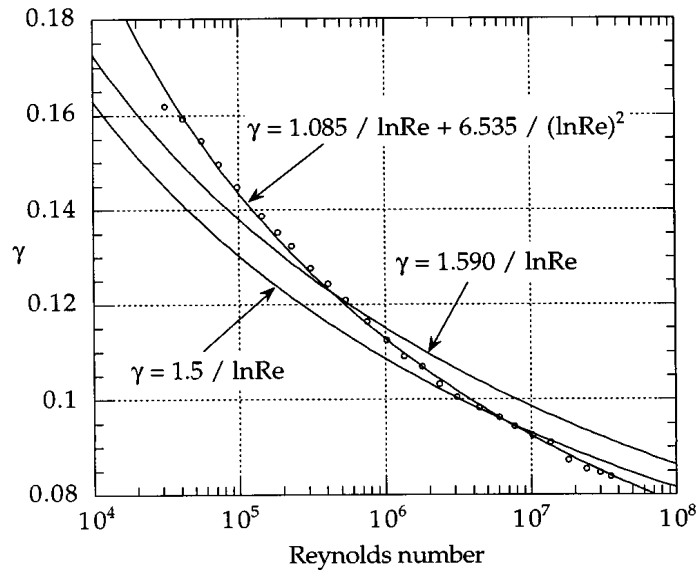
$Re = 3.1 \times 10^6$

0×10^3

$Re = 35 \times 10^6$

$10^2 \quad 10^3 \quad 10^4 \quad 10^5 \quad 10^6$

y^+

$Re = 310 \times 10^3$

$Re = 31 \times 10^3$

$Re = 35 \times 10^6$

U^+

$10^0 \quad 10^1 \quad 10^2 \quad 10^3 \quad 10^4 \quad 10^5 \quad 10^6$

y^+

$\gamma = 1.083 \; / \; \ln Re + 6.553 \; / \; (\ln Re)$

γ

$\gamma = 1.590 \; / \; \ln Re$

$\gamma = 1.5 \; / \; \ln Re$

$10^4 \quad 10^5 \quad 10^6 \quad 10^7 \quad 10^8$

Reynolds number

FIG. 7. Plot of the exponent in the power law given by Eq. (10) for 26 different Reynolds numbers between 31×10^3 and 35×10^6.

$C = 0.577 \; \ln Re + 2.5$

C

$C = 0.7053 \; \ln Re + 0.3055$

$10^4 \quad 10^5 \quad 10^6 \quad 10^7 \quad 10^8$

Reynolds number

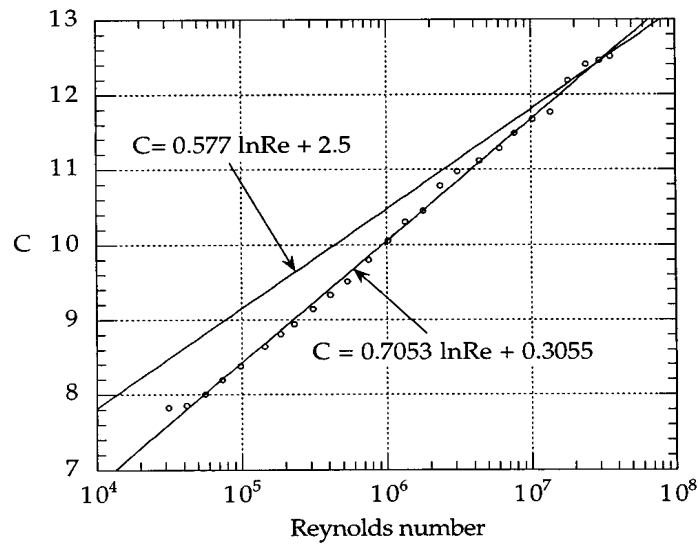FIG. 6. Plot of the multiplicative constant in the power law given by Eq. (10) for 26 different Reynolds numbers between 31×10^3 and 35×10^6.
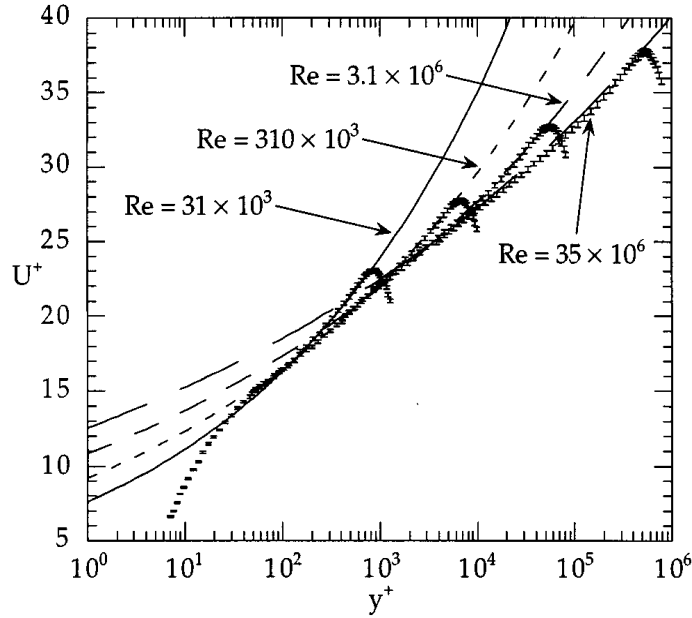

$Re = 3.1 \times$

$Re = 310 \times 10^3$

$Re = 31 \times 10^3$

U^+

$10^0 \quad 10^1 \quad 10^2 \quad 10^3$

y^+

$C = 0.577 \; \ln Re + 2.5$

$C = 0.7053 \; \ln Re + 0.3055$

$Re = 310 \times 10^3$

$Re = 31 \times 10^3$

$Re = 35 \times 10^6$

U^+

$10^0 \quad 10^1 \quad 10^2 \quad 10^3 \quad 10^4 \quad 10^5 \quad 10^6$

73

$C = 0.7053 \ln Re + 0.3055$

+ 2.5

$10^6 \qquad 10^7 \qquad 10^8$

Reynolds number

Re = 3.1 × 10⁶

Re = 310 × 10³

Re = 31 × 10³

Re = 35 × 10⁶

U^+

y^+

FIG. 8. Comparison between the mean velocity profiles and Eq. (15) for 4 different Reynolds numbers between 31×10^3 and 35×10^6. The error bars represent an uncertainty in U^+ of $\pm 0.57\%$.

Zagarola, Perry, and Smits

Barenblatt & Chorin in

> G. I. Barenblatt & A. J. Chorin, "Scaling of the intermediate region in wall-bounded turbulence: the power-law," Phys. Fluids **10** 1043-1044 (1998)

have imputed the disagreement with the Superpipe data at the higher Reynolds numbders to the effects of roughness, which should become more important as Re increases. The issue of roughness has been addressed by

> M. A. Shockling, J. J. Allen & A. J. Smits, "Roughness effects in turbulent pipe flow," J. Fluid Mech. **564** 267-285 (2006)

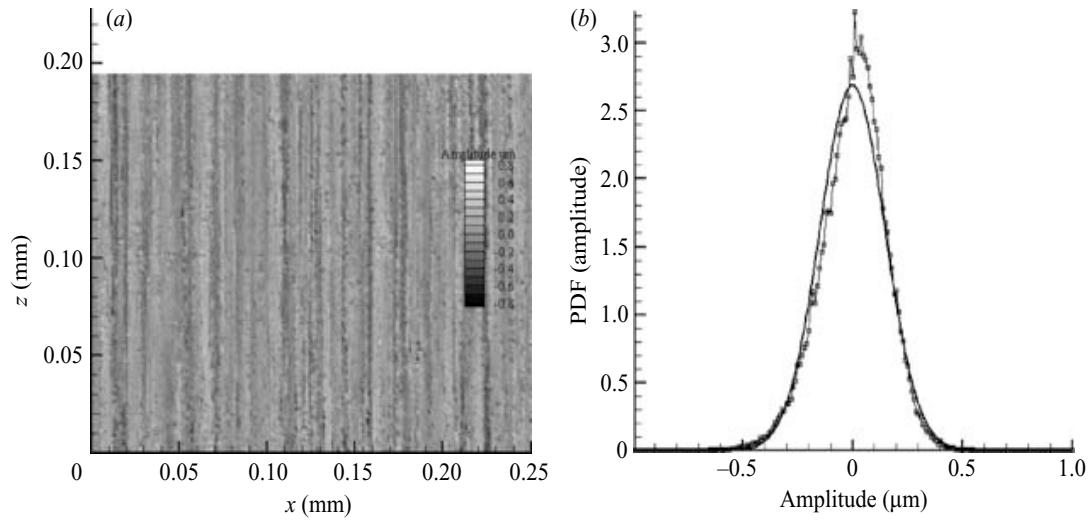By performing new experiments with increased k^+, the effects of roughness were systematically studied.

74

FIGURE 2. (*a*) Two-dimensional surface plot of the original Superpipe. Area shown is about 0.2 mm × 0.25 mm, and the amplitudes are in μm. (*b*) Probability density function of surface elevation.
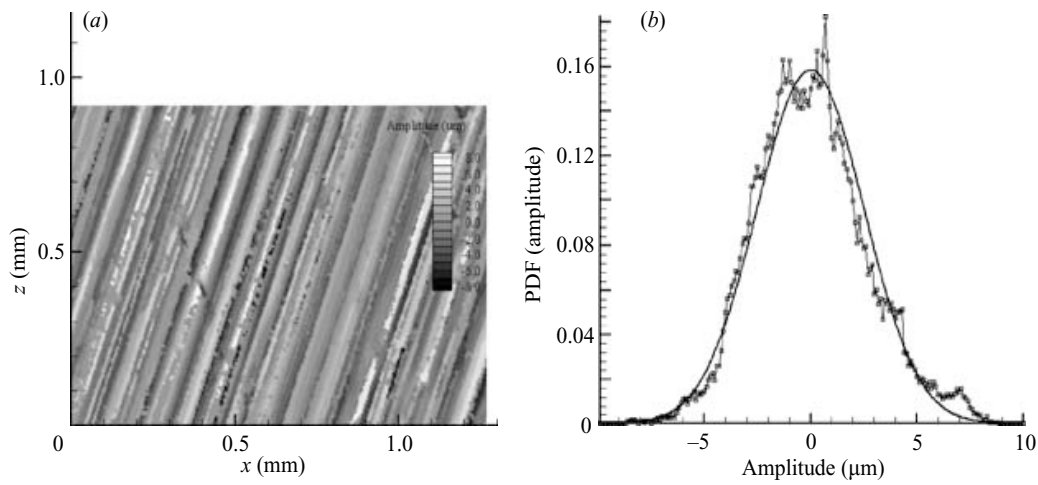
FIGURE 3. (*a*) Two-dimensional surface plot of the new rough pipe. Area shown is about 0.8 mm × 1.2 mm, and the amplitudes are in μm. (*b*) Probability density function of surface elevation.

A first result is shown for the friction factor $\lambda = 8(u_*/\bar{u}_m)^2$, which shows no effects of roughness for $Re < 10^6$, in agreement with original claims of Zagarola & Smits. The friction coefficient is non-monotonic in the Reynolds number, showing a "belly" qualitatively similar to that seen in the old data of Nikuradze.
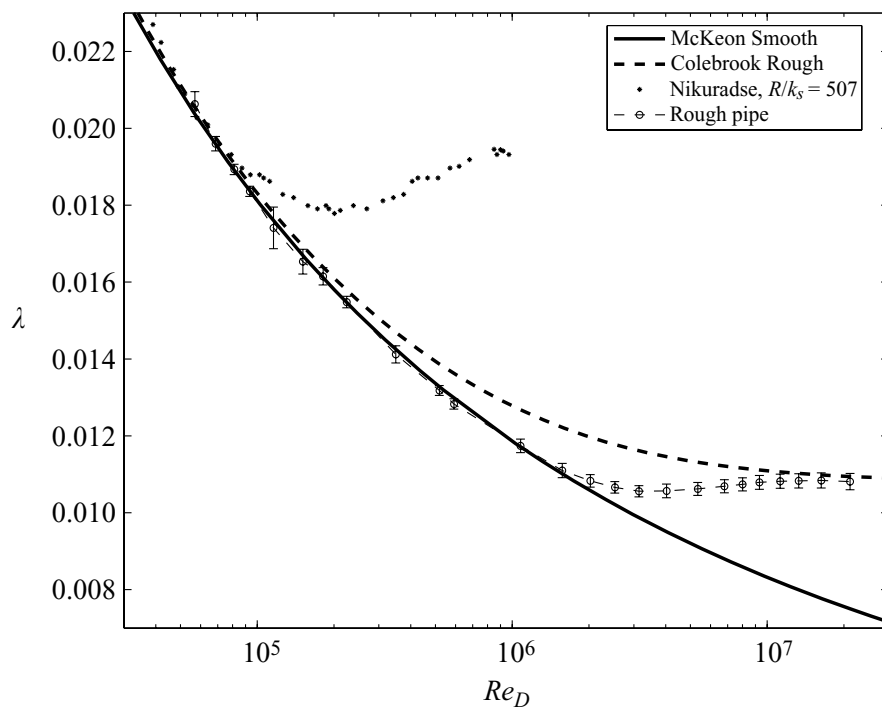
FIGURE 6. Friction factor λ for the present surface, compared with the rough-all relations of Colebrook (1939) for the same k_s, the smooth-wall relation of McKeon *et al.* (2005) (equation (2.4)), and the results for the smallest sandgrain roughness used by Nikuradse (1933).

Shockling et al. have also studied the downward velocity profile shift with roughness, which has been observed in previous studies as well. There are no effects of roughness in the new rough pipe for $k_s^+ < 3.5$, again bolstering their previous claims about the lack of roughness effects in the smooth-pipe experiment.
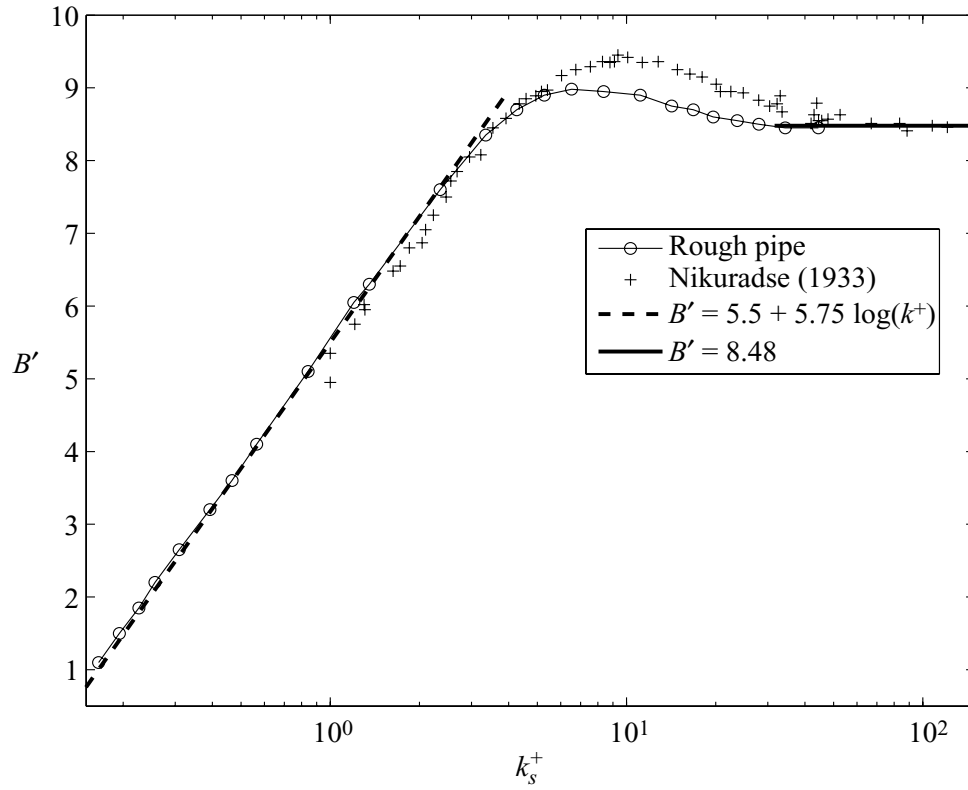
FIGURE 16. The velocity profile shift according to Nikuradse's roughness scaling, showing smooth, transitional, and fully rough regimes.

Finally, Shockling et al. have verified Townsend's "outer layer similarity hypothesis," which states that there should be no effect of roughness in the outer layer, except for the change in friction velocity u_k. The authors observe excellent scaling of the velocity profiles in outer scaling for the smooth and rough pipe experiments.
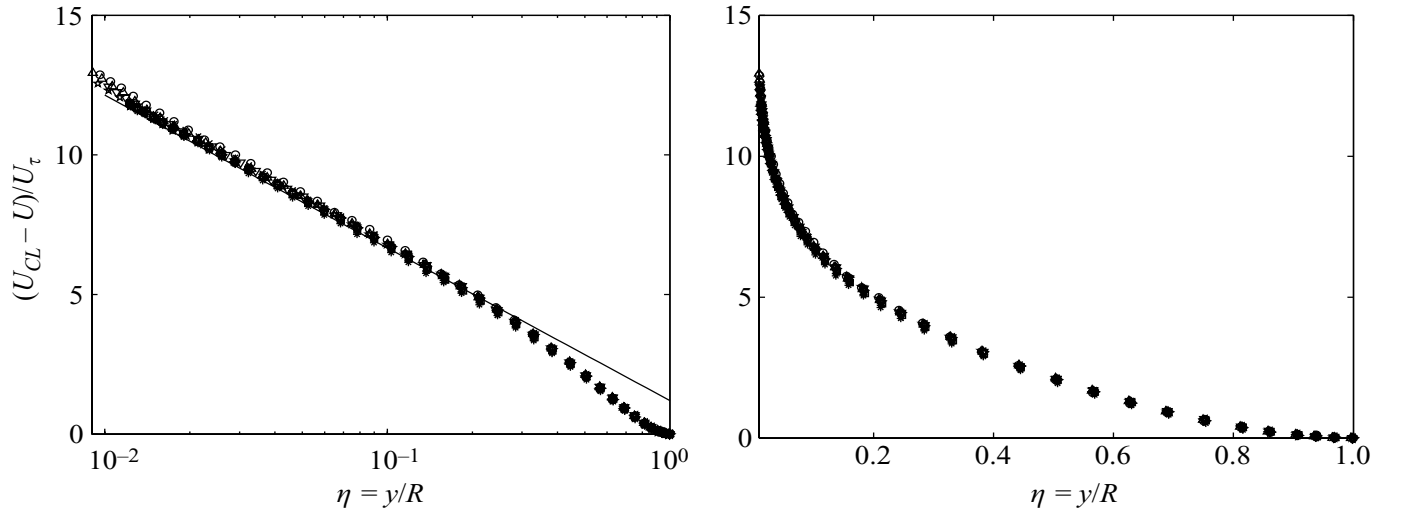

FIGURE 17. Outer scaling for $349 \times 10^3 \leqslant Re_D \leqslant 21.2 \times 10^6$. Solid line: $-(1/0.421)\ln\eta + 1.20$.